PERGAMON

International Journal of Heat and Mass Transfer 45 (2002) 4069–4078

International Journal of HEAT and MASS TRANSFER

www.elsevier.com/locate/ijhmt

Local heat transfer measurements of plate finned-tube heat exchangers by infrared thermography

Herchang Ay [a,*], JiinYuh Jang [b], Jer-Nan Yeh [b]

[a] Department of Mechanical Engineering, Southern Taiwan University of Technology, Tainan 71005, Taiwan
[b] Department of Mechanical Engineering, National Cheng-Kung University, Tainan 70101, Taiwan

Received 2 November 2001; received in revised form 26 March 2002

Abstract

An experimental study is performed using an infrared thermovision to monitor temperature distribution over a plate-fin surface inside the plate finned-tube heat exchangers. The differentiation of the temperature function is derived to determine the local convective heat transfer coefficients on the tested fin, using a local element lumped conduction equation included the convective effect on the boundaries with experimental data. It is disclosed that the infrared thermography is capable of rapidly detecting location and extent of transition and separation regions of the boundary layer over the whole surface of the tested models. Through the comparison of the test results on the strategy region of the in-line and staggered arrangements, it is more easy to understand or interpret the detailed dynamic phenomena of flow existed in the heat exchangers. In addition, the experimental results demonstrate that the averaged heat transfer coefficient of staggered configuration is 14–32% higher than that of in-lined configuration

1. Introduction

The heat exchanger is an essential unit in heat extraction and recovery systems. With increasing emphasis on energy savings, efforts are being made to develop better heat transfer surfaces for more efficient heat transfer equipment. Various types of heat transfer surfaces have been introduced in Kays and London [1]. However, the estimation of convective heat transfer coefficients and/or heat flux rates from a surface is of particular importance to design a new heat transfer surface for high-performance heat exchangers. Unfortunately, measurement of the convective heat transfer coefficient is more difficult to perform than other common thermo-fluid-dynamic quantities, especially in case of non-uniform distributions and/or of conduction–convection problem. Usually, measuring heat fluxes involves measuring temperatures [2]. In particular, when considering two-dimensional problems, the starting point is generally the knowledge of surface temperature distribution in the system. An infrared thermographic system is developed as an effective tool for measurement of surface temperature distribution and for heat flux restoration due to its high spatial and temporal resolution, high sensitivity, and non-invasive nature.

In recent years, a number of studies have been published on infrared thermography in heat transfer and flow visualization. Simeonides et al. [3] and Henckels et al. [4] developed the infrared thermographic technique in the measurement of heat transfer in a hypersonic tunnel. de Luca et al. [5] employed a computerized infrared scanning radiometer to characterize the boundary layer development over a model wing, having a Göttingen 797 cross-section, by measuring the temperature distribution over its heated surface. Cardone et al. [6] investigated the flow produced by a flat disk rotating in still air by an infrared camera. Ay [7] and Ay and Yang [8] employed an infrared thermovision to visualize and simultaneous, real-time thermal-image processing in the global temperature distribution over the surfaces of the cutting tool, workpiece and chip.

* Corresponding author. Tel.: +886-6-2533131; fax: +886-6-2425092.
E-mail address: herchang@mail.stut.edu.tw (H. Ay).

0017-9310/02/$ - see front matter
PII: S0017-9310(02)00132-1

Nomenclature

A	the control surface area of the fin (mm^2)
D_o	outside diameter of the tube (mm)
f	friction factor
h	the local convective heat transfer coefficient ($W/m^2\,°C$)
$\bar{h}$	the averaged convective heat transfer coefficient ($W/m^2\,°C$)
H	fin spacing (mm)
j	Colburn factor
k	thermal conductivity($W/m\,°C$)
L	length of the test section (mm)
ℓ	length of the imaging element (mm)
q	heat flux (W/m^2)
Re	Reynolds number, UH/v
t_f	thickness of the fin (mm)
t_u	thickness of the tube (mm)
T	temperature (°C)
T_m	measurement fin temperature through a transparent sheet (°C)
T_r	real fin temperature (°C)
T_w	local wall temperature of the fin surface (°C)
T_∞	bulk mean temperature of the stream (°C)
U	frontal velocity (m/s)
W	width of the test section (mm)
x	x-direction coordinate
X	imaging pixel in x coordinate
X_t	transverse pitch (mm)
X_l	longitudinal pitch (mm)
y	y-direction coordinate
Y	imaging pixel in y coordinate

Greek symbols

δ	thickness of fin (mm)
ε	emissivity
v	kinematic viscosity (m^2/s)

Available experimental information on the plate-fin and tube heat exchangers have been presented, reviewed and correlated in the open literatures. Saboya and Sparrow [9–11] used the naphthalene mass transfer method to measure the local coefficients for one-, two- and three-row plate-fin and tube heat exchangers. Rich [12,13] investigated the effects of fin-pitch and number of tube row for staggered plate-fin and tube heat exchangers. Correlations to predict the Colburn (j) and friction factor (f) vs. Reynolds number for plain fins on staggered tubes were developed by McQuistion [14] and Gray and Webb [15]. McQuistion and Parker [16] collected a lot of the experimental data up to 1994 in a book.

The aim of the present study is to show that it is possible to record the temperature distribution on a plate-fin inside the plate finned-tube heat exchangers with the advanced infrared thermovision system. Two typical plate finned-tube heat exchangers, in-line and staggered tube arrangements, were tested under various frontal velocities. In addition, the local convection heat transfer coefficients over the fin are determined by means of a control volume based finite difference formulation after the temperature value identified over the tested surface.

2. Experimental equipment and procedure

2.1. Experimental apparatus

The experimental setup, as schematically illustrated in Fig. 1, used to investigate the local heat transfer performance of a plate consisted of a three-row plate-fin and tube heat exchanger situated in a subsonic blow-down open-circuit wind tunnel. The wind tunnel consisted of an axial flow, diffusers, a settling chamber, construction sections, test section, and provides an approach velocity that is flat to within one percent, with a turbulent intensity less than one percent. The airflow is driving by the 5.6 kW (7.5 h.p.) axial flow fan with an inverter to adjust the output power. Eight type-K thermocouples are mounted at the corners of the center test core; four each on the inlet and outlet section of the tested model. The data signals are individually recorded and then averaged. During the isothermal test, the random fluctuation of these thermocouples is within ± 0.2 °C. In addition, all thermocouples are pre-calibrated by a quartz thermometer with 0.01 °C precision.

2.2. Test model

The test section, shown schematically in Fig. 2(a), is constructed of stainless steel for large scale testing of a bank of tubes shared continuous plate-fins. Both of in-line and staggered tube arrangements are used in this study. Fig. 2(b) and (c) are the description of coordinate systems and nomenclature for the tested fins. There are six different staggered and in-lined test sections for the present experimental investigation. Their detailed geometrical parameters are tabulated in Table 1. Each tube is locally heated by means of joulean dissipation in a wire inserted in the central region of a cylinder installed in the tube. Electric power is supplied to the heater

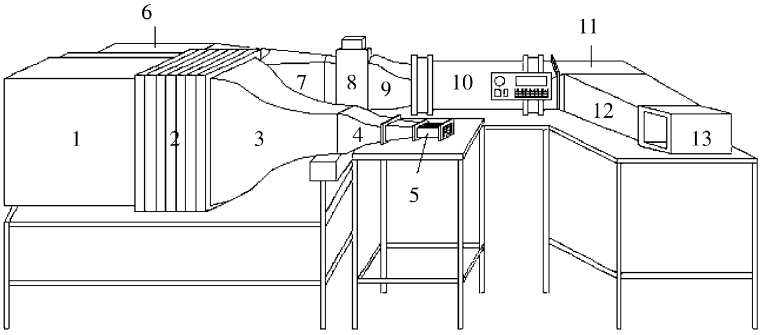

1: corner
2: settling chamber
3: contraction section (contraction area ratio:10.17:1)
4. contraction section
5: test section
6: corner
7: diffuser
8: heater, removable rack
9: C/R transition section
10: fan, power section
11: corner
12: diffuser
13: corner

Fig. 1. Schematic diagram of the experimental setup.

through cables from a GW GPS-3030 DC power supply (0–30 V, 0–3 A). The surface of the fin is coated on both sides with thin film of opaque paint with emissivity (ε) of 0.95. In order to measure the temperature distribution on the surface of plate-fin inside test core by an infrared camera, a transparent sheet, Fig. 2(a), replaces the top plate-fin of the test core. A portion of the thermal electromagnetic radiation emitted by the test fin will absorb and reflect on the transparent sheet. Before the experimental tests of the infrared temperature measurement, it is necessary to measure the temperature on strategy area of a heating fin through with and without the transparent sheet. This calibration is perform is rather linear, as shown in Fig. 3, for the tested temperature ranges.

2.3. Infrared system thermovision

The experimental apparatus for infrared temperature measurements used in AGEMA Themovision 550 (THV550). The sensing system of THV550 is a focal plane array (FPA) detector made of a matrix with 320 (H) $\times$ 240 (V) PtSi elements. The electromagnetic energy radiated in the infrared spectral band by an object will convert into an electronic signal from all the sensors and acquire simultaneously in the whole field of view. The field of view depends on the optics focal length and on the viewing distance. Thermal images can be captured at a frequency the many of up to 60 frames per second and the thermography is digitally recorded with a 12-bit dynamic range. According to the manufacturer, the accuracy is $\pm 2\%$, the spatial resolution 1.1 mrad (IFOV) and the thermal sensitivity <0.1 °C at 30 °C. Before the experimental tests, it is necessary to provide the object parameters, including the emissivity, object distance, relative humidity, atmospheric temperature, and reflected ambient temperature, for the system performance.

2.4. Experimental procedure

For testing, the fan was started. The desired air velocity through the test section was set by means of adjusting an inverter. The frontal air velocity, U, was measured by a hot wire with $\pm 2.0\%$ accuracy. Nine power supplies were turned on and adjusted to bring the outside wall temperature of nine tubes to 60 °C, respectively. When steady state values had been established, the temperature map of the plate-fin surface was

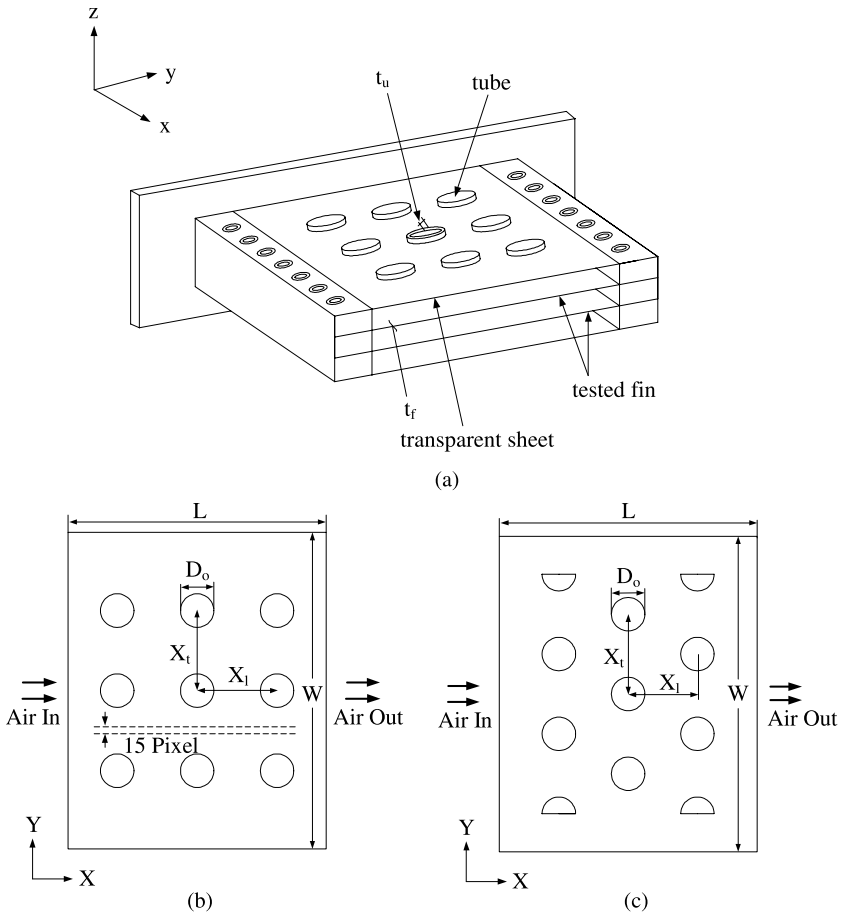

Fig. 2. The experimental test models: (a) schematic of the wind tunnel test section, and sketch illustrating nomenclature for (b) in-line tube arrangements, and (c) staggered tube arrangements.

Table 1
Geometrical parameters of the test sections

Tube arrangement / Test section	In-line			Staggered		
	1	2	3	4	5	6
H (mm)	10	15	20	10	15	20
L (mm)		196			196	
W (mm)		240			240	
D_o (mm)		25.4			25.4	
X_l (mm)		60.7			52.6	
X_t (mm)		60.7			60.7	
t_u (mm)		2.0			2.0	
t_f (mm)		0.5			0.5	
Tube number		9			9	
Row number		3			3	

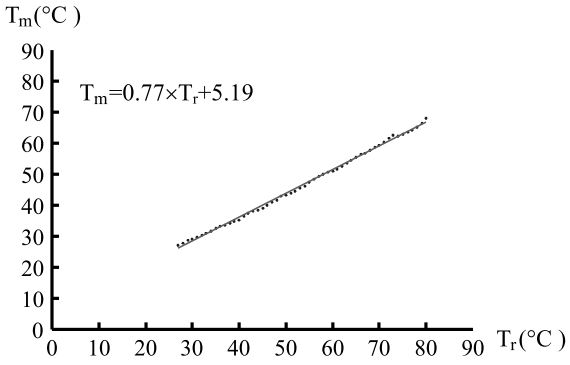

Fig. 3. IR camera calibration curve.

recorded. The imaging size of the map was a plane matrix array with 220 pixels × 220 pixels for in-lined and 194 pixels × 246 pixels for staggered arrangements. Following the temperature value identified at each pixel by the infrared thermovision system, the local convective heat transfer coefficients over the fin were determined by means of a control volume based finite difference formulation. For steady conduction we consider the ener-

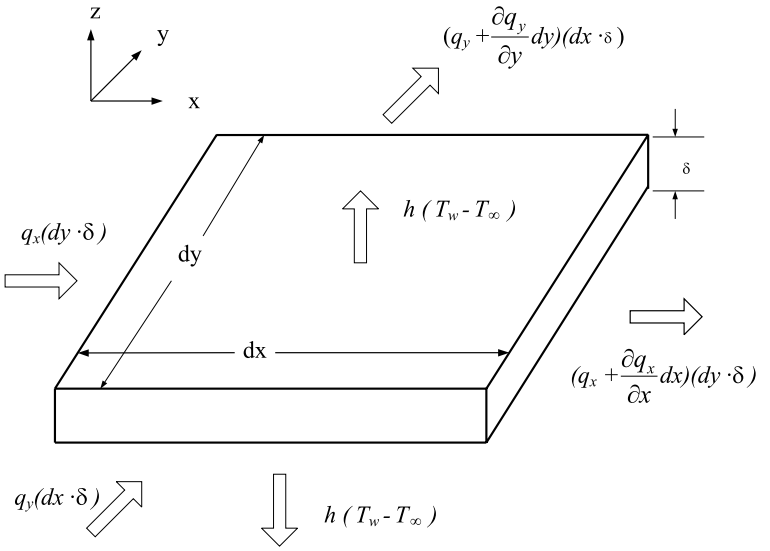

Fig. 4. Differential control volume for three-dimensional conduction with heat dissipation by convection in rectangular coordinates.

gy-balance equation for a small control volume illustrated in Fig. 4, stated as

$$2h(T_w - T_\infty)\mathrm{d}x\,\mathrm{d}y = -\frac{\partial q_x}{\partial x}\,\mathrm{d}x\mathrm{d}y\delta - \frac{\partial q_y}{\partial y}\mathrm{d}x\,\mathrm{d}y\delta \tag{1}$$

where δ is the thickness of the fin and T_∞ is the bulk mean temperature of the stream. A uniform temperature on the plate along the z-direction is assumed in Eq. (1) due to the Biot number based on δ estimated about 10^{-3}. In terms of Fourier's law,

$$q_x = -k\frac{\partial T}{\partial x}, \quad q_y = -k\frac{\partial T}{\partial y} \tag{2}$$

The substitution of Eq. (2) into Eq. (1) yields

$$h = \frac{k\delta}{2(T_w - T_\infty)}\left(\frac{\partial^2 T}{\partial x^2} + \frac{\partial^2 T}{\partial y^2}\right) \tag{3}$$

The control volume approach was used to discretize the derivatives in Eq. (3) given by

$$h = \frac{k\delta}{2(T_{x,y} - T_\infty)}\left(\frac{T_{x+1,y} - 2T_{x,y} + T_{x-1,y}}{\Delta x^2} + \frac{T_{x,y+1} - 2T_{x,y} + T_{x,y-1}}{\Delta y^2}\right) \tag{4}$$

If we assume a square mesh $\Delta x = \Delta y = \ell$, Eq. (4) simplifies to

$$h = \frac{k\delta}{2(T_{x,y} - T_\infty)}\left(\frac{T_{x+1,y} + T_{x-1,y} + T_{x,y+1} + T_{x,y-1} - 4T_{x,y}}{\ell^2}\right) \tag{5}$$

Here, ℓ is the length of the imaging element (pixel) estimated as 0.77 mm in the thermograms. Using Eq. (5), a conservatively, and estimated uncertainty of ±7.0% for the buck mean temperature of fluid, T_∞, and the uncertainty estimation method of Kline and McClintock [17], the maximum uncertainty of the calculated the local convective heat transfer coefficient is ±7.5%.

The averaged heat transfer coefficient, $\bar{h}$, then can be obtained by

$$\bar{h} = \frac{1}{A}\int_A h\,\mathrm{d}A \tag{6}$$

where $\mathrm{d}A$ is the control surface element of the fin and defined as $\mathrm{d}x \times \mathrm{d}y$ in Fig. 4. The uncertainty in the averaged heat transfer coefficient is ±7.6% estimated by the similar method [17]. Note that the highest uncertainties are associated with lower Reynolds number.

3. Experimental results and discussion

The results of the infrared thermovision for steady-state temperature distribution on the plate-fin surface of the middle test core with fin spacing $H = 10$ mm for three different frontal velocity $U = 0.5$, 1.0, 1.5 m/s are presented in Figs. 5–7 which include the in-line arrangement in part (a) and the staggered arrangement in part (b). The associated local convective heat transfer coefficient maps are shown in Figs. 8–10. Each tube of the test models is subjected to a heat flux and keeping the wall temperature of tube 60 °C. A 20-step color palette for thermograms (≈1.1 °C per step) and for the local convective coefficients (≈0.95 W/m^2 °C per step) maps are used in these figures, so that temperatures or

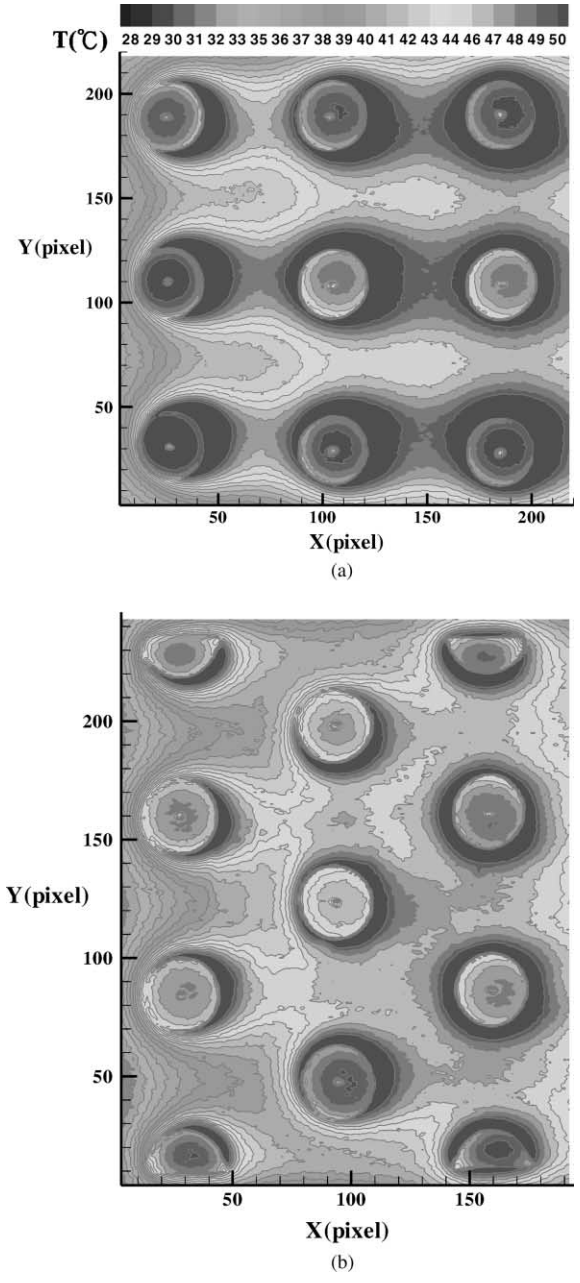

Fig. 5. Steady-state temperature distribution on the plate-fin surface (a) in-line, (b) staggered arrangement for $H = 10$ mm, and $U = 0.5$ m/s.

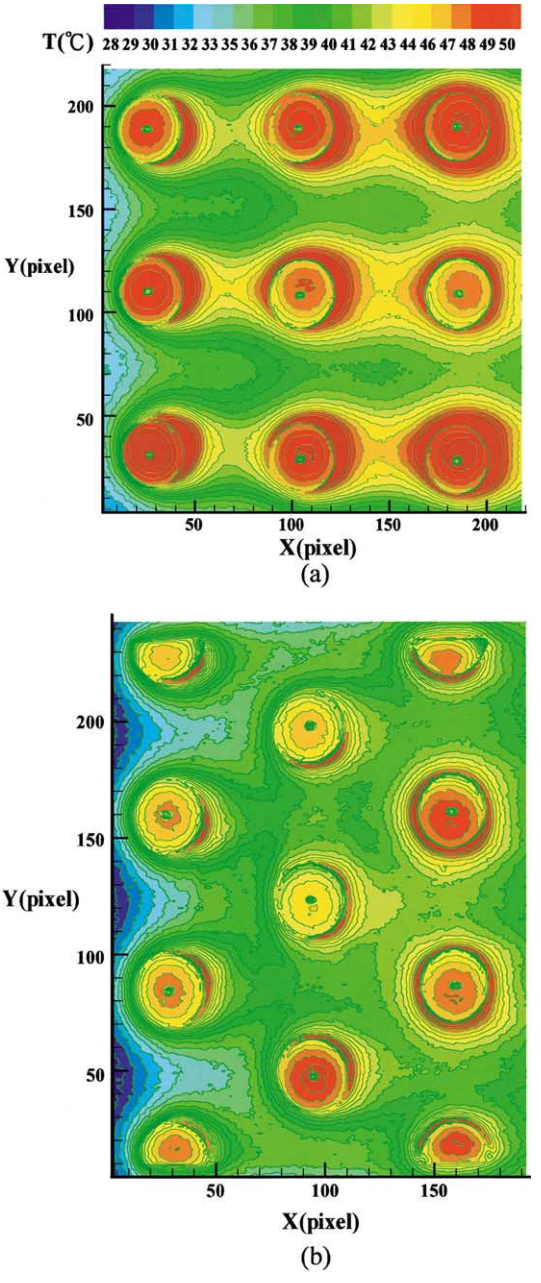

Fig. 6. Steady-state temperature distribution on the plate-fin surface (a) in-line, (b) staggered arrangement for $H = 10$ mm, and $U = 1.0$ m/s.

local convective coefficients throughout the plate-fin surface can easily be correlated.

At the leading edge of the plate-fin, the results indicate lower temperature, as shown in Figs. 5–7, and consistently higher convective heat transfer coefficient of Figs. 8–10, because the velocity boundary layer is initially developed in the z-direction. A most pronounced effect is that the temperature gradient on the fin surface is sharper near the front and sides of the first two row tubes due to the repeated growth and destruction of the boundary layer by tubes. However, at the rear of the tube, the temperature gradient is gentler because the airflow is swept downstream into the wake. A different characteristic occurs after the third row due to an ad-

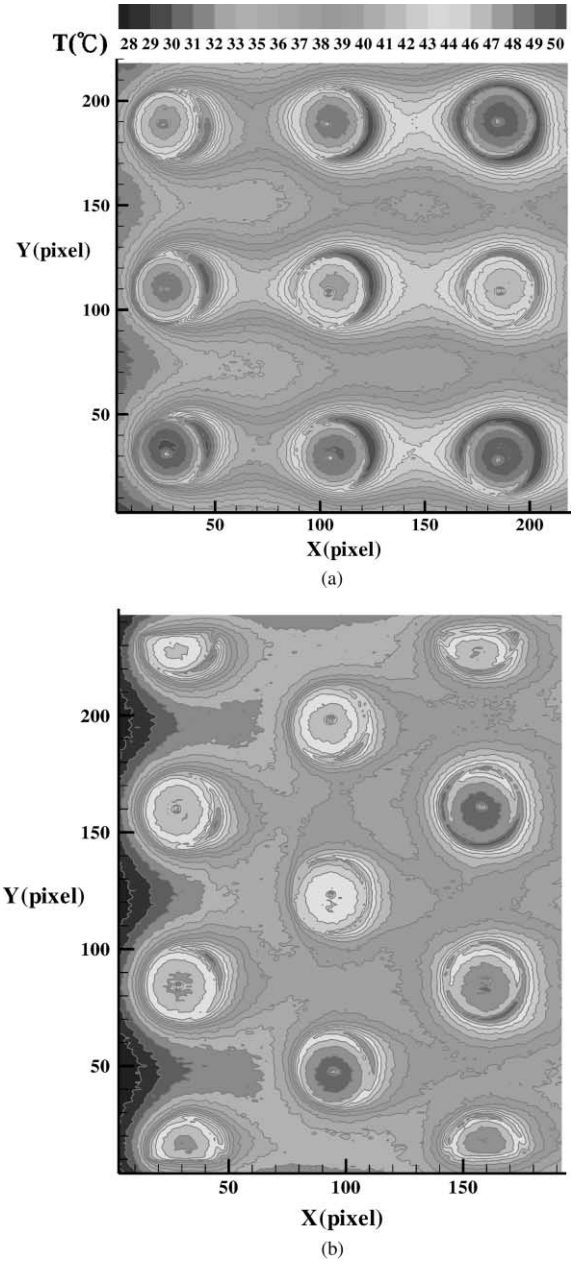

Fig. 7. Steady-state temperature distribution on the plate-fin surface (a) in-line, (b) staggered arrangement for $H = 10$ mm, and $U = 1.5$ m/s.

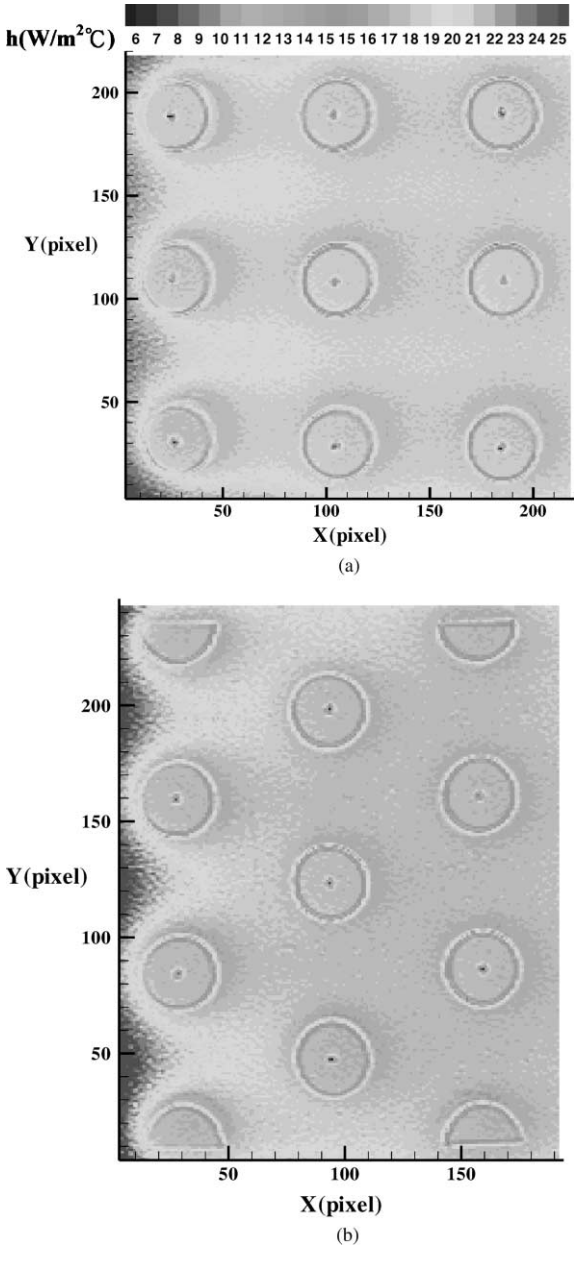

Fig. 8. Local convective heat transfer coefficients on the plate-fin surface (a) in-line, (b) staggered arrangement for $H = 10$ mm, and $U = 0.5$ m/s.

ditional exit effect. The wake region is greater for smaller frontal velocities, and appears asymmetric pattern even at lower Reynolds numbers. For a closed spaced staggered-tube arrangement, the wake behind each tube is somewhat smaller than for similar in-line arrangements. These phenomena can also be obvious from relative thermograms and local convective coefficients maps. By comparing Figs. 5–7, one can see that the temperature gradient around the tubes increases as the frontal velocity increases and the local convection coefficient is obviously increased as referring to Figs. 8–10.

Fig. 11 illustrates the variation of the span-averaged convective coefficients along the downstream direction between the transverse tubes with fin spacing

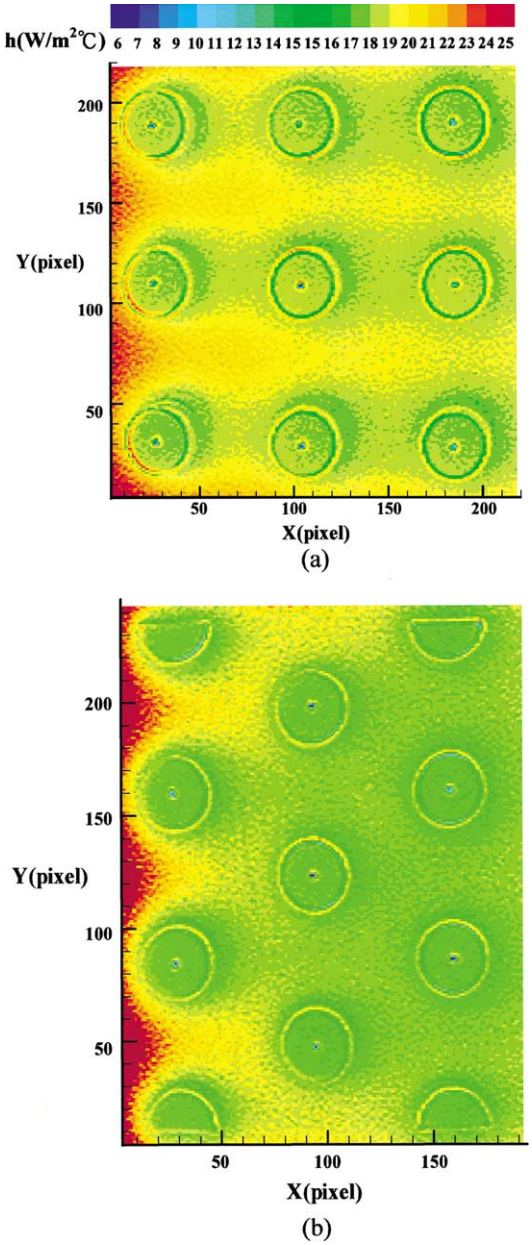

Fig. 9. Local convective heat transfer coefficients on the plate-fin surface (a) in-line, (b) staggered arrangement for $H = 10$ mm, and $U = 1.0$ m/s.

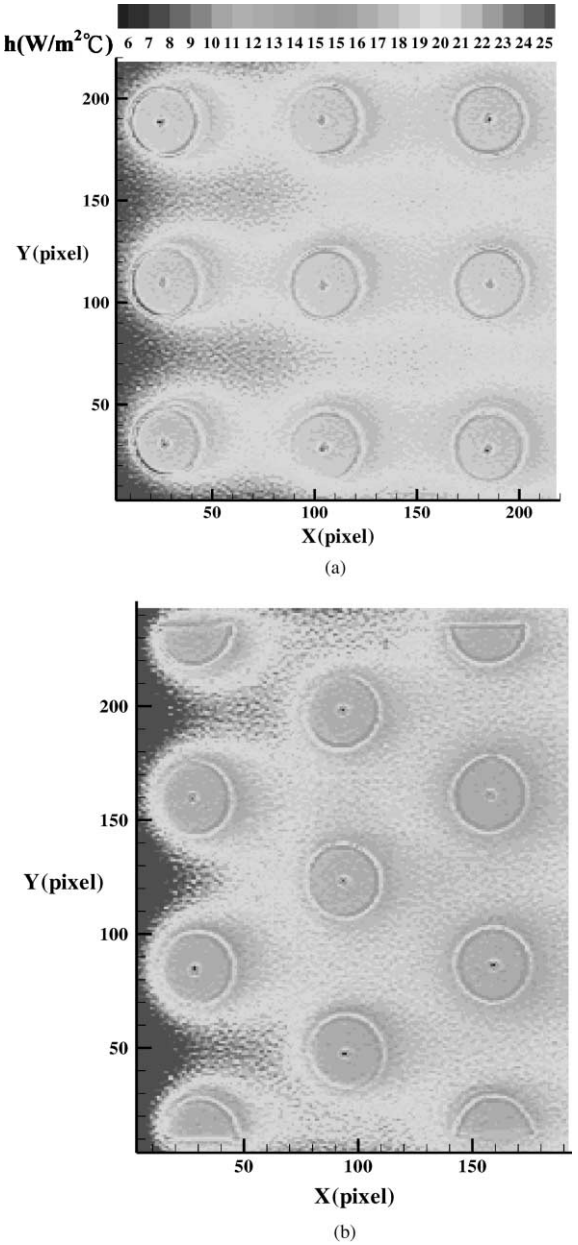

Fig. 10. Local convective heat transfer coefficients on the plate-fin surface (a) in-line, (b) staggered arrangement for $H = 10$ mm, and $U = 1.5$ m/s.

$H = 20$ mm for the in-line array. The coordinate X, is measured from the leading edge of the test fin surface (see Fig. 2), and indicated the imaging pixel (1 pixel = 0.77 mm). For each point on the plot (at a fixed position in X), 15 pixels widths are taken in the spanwise (Y) direction and averaged. At a relatively low Reynolds number, $Re = 543$, the local convective coefficients (h) decrease along with the distance from the inlet due to the development of a boundary layer in the thermal entrance. After the first row, a tardily decreasing h towards the outlet edge of the fin because a thermally fully developed region initially occurs at this location. Also in this case, a slight fluctuation of h-value can be seen in adjacent longitudinal rows, since the varied free-flow area may induce different wake forming behind tubes. For low velocity flow, it is noted that the shape of

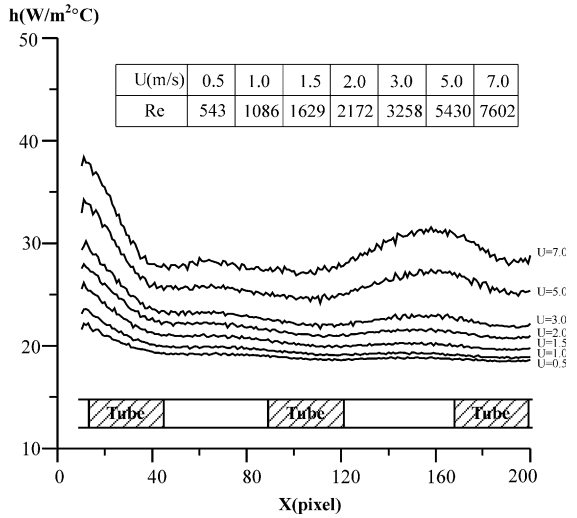

Fig. 11. The variations of the span-averaged local convective coefficients with $H = 20$ mm for the in-line array.

h-variation is preserved even though its amplitude may vary in the longitudinal direction. The entrance effect is also existed in all of the test cases shown in Fig. 11, just similar to that of the pipe flow. For the Reynolds numbers exceeded 2172, nevertheless, the h distribution shows a substantially different pattern after the first row. At $Re = 3258$, the convective coefficient increases with the distance, reaching a maximum between adjacent tubes in the first two rows, and then decreases to reach a minimum at the second row. This h behavior repeats after the second row, then exhibiting a higher maximum h near the frontal face of the third row. It should be noted that the h increases more sharply near the third row, with a combination of the turbulent effect and the exit effect at the third row. In addition, the deviation in the h curve rises with an increase in the Reynolds number. For example, in the case of $Re = 7602$, the deviation becomes very large.

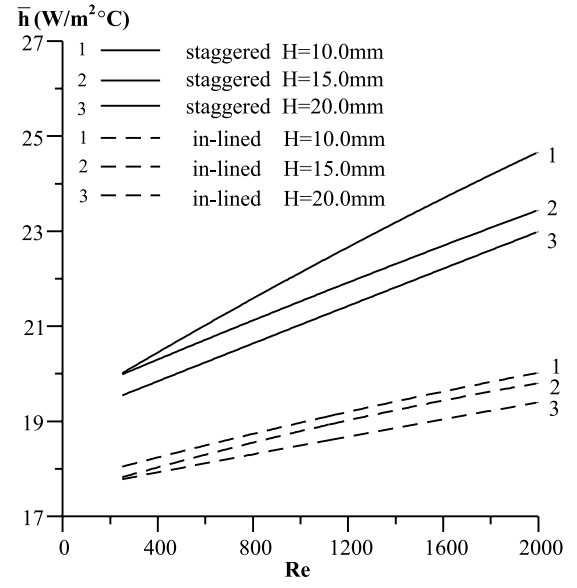

Fig. 12. A comparison of the averaged convective heat transfer coefficients under $U = 1$ m/s.

Fig. 12 shows a comparison of the averaged convective heat transfer coefficients ($\bar{h}$) on a fin at various Reynolds numbers ranging from 543 to 2172 under the test condition of $U = 1$ m/s, $H = 20$ mm. The solid and dashed lines represent the results for the staggered and in-line arrays, respectively. It is seen that the averaged heat transfer coefficients of staggered arrangement is 14–32% higher than that of in-line arrangement.

4. Conclusion

An infrared thermovision has been employed to visualize and quantitatively evaluate in the global temperature distribution over the fin surface inside a plate-finned-tube heat exchanger. Following the temperature value identified at each pixel, the local convective heat transfer coefficients over the fin are determined by means of a control volume based finite difference formulation. The results show that the infrared thermography is capable of rapidly detecting location and extent of transition and separation regions of the boundary layer over the whole surface of the test model. Through the comparison of the test results on the strategy region of the in-line and staggered arrangements, it is more easy to understand or interpret the detailed dynamic phenomena of flow existed in the heat exchangers.

For the in-line array, the shape of the span-averaged convective coefficient profile on the fin surface along the downstream direction between the transverse tubes is similar to that of the pipe flow, and exhibited the meniscus at the end of a liquid column in capillary while the Reynolds numbers less than 2172. Whereas, if the Reynolds numbers is higher than 3258, the results show a gigantic waviness in the local convective coefficient curves. Finally, the experimental results demonstrate that the averaged heat transfer coefficient of staggered configuration is 14–32% higher than that of in-lined configuration.

Acknowledgements

This research is supported by the National Science Council of Taiwan under contract NSC 89-2212-E-006-131 and NSC 88-2511-S-218-002. The authors are indebted to Mr. C.-F. Liang, K.-B. Sun, H.-C. Wang and

C.-H. Chou for the experimental setup participated through their related work.

References

[1] W.M. Kays, A.L. London, Compact Heat Exchangers, third ed., McGraw-Hill, New York, 1984.
[2] G.M. Carlomagno, thermo-fluid-dynamic application of quantitative infrared thermography, in: S. Mochizuki (Ed.), Proceedings of the First Pacific Symposium on Flow Visualization and Image Processing, Honolulu, 1997, p. 35–44.
[3] G. Simeonides, P. Van Lierde, S. Van der Stichele, D. Capriotti, J.F. Wendt, Infrared thermography in blow-down and intermittent hypersonic facilities, AIAA paper 89-0042 (1989).
[4] A. Henckels, F. Maurer, H. Olivier, H. Grönig, Fast temperature measurement by infrared line scanning in a hypersonic shock tunnel, Expt. Fluid. 9 (1990) 298–300.
[5] L. de Luca, G.M. Carlomagno, G. Buresti, Boundary layer diagnostics by means of an infrared scanning radiometer, Expt. Fluid. 9 (1990) 121–128.
[6] G. Cardone, T. Astarita, G.M. Carlomagno, IR heat transfer measurements on a rotating disk, in: D. Balageas, G. Busse, G.M. Carlomagno (Eds.), QIRT 94, Eurotherm series 42, EETI, 1994.
[7] H. Ay, Heat Transfer and Life of Cutting Tool in Turning, Ph.D. thesis, University of Michigan, Ann Arbor, MI, 1995.
[8] H. Ay, W.-J. Yang, Heat transfer and life of metal cutting tools in turning, Int. J. Heat Mass Transfer 22 (3) (1998) 613–623.
[9] F.E.M. Saboya, E.M. Sparrow, Local and average transfer coefficients for one-row plate fin and tube heat exchanger configurations, ASME J. Heat Transfer 96 (1974) 265–272.
[10] F.E.M. Saboya, E.M. Sparrow, Transfer characteristics of two row plate fin and tube heat exchanger configurations, Int. J. Heat Mass Transfer 19 (1976) 41–49.
[11] F.E.M. Saboya, E.M. Sparrow, Experiments on a three-row fin and tube heat exchanger, J. Heat Transfer 19 (1976) 26–34.
[12] D.G. Rich, The effect of fin spacing on the heat transfer and friction performance of multi-row plate fin-and-tube heat exchangers, ASHRAE Trans. 17 (1973) 137–145.
[13] D.G. Rich, The effect of the number of tube rows on the heat transfer performance of smooth plate and fin-and-tube heat exchangers, ASHRAE Trans. 81 (1975) 307–317.
[14] F.C. McQusiston, Correlation for heat, mass and momentum transport coefficients for plate-fin-tube heat transfer surfaces with staggered tube, ASHRAE Trans. 84 (1978) 294–309.
[15] D.L. Gray, R.L. Webb, Heat transfer and friction correlations for plate fin-and-tube heat exchangers having plain fins, Proceedings of the Nineth International Heat Transfer Conference, San Francisco, 1986.
[16] F.C. McQuiston, J.D. Parker, Heating, Ventilating And Air Conditioning Analysis and Design, John Wiley, New York, 1994.
[17] S.J. Kline, F.A. McClintock, Describing uncertainties single-sample experiments, Mech. Eng. 75 (1953) 3–8.